Tire-Road Friction Estimation based on Frequency Characteristics of In-Wheel Electric Drive System

Conference Paper · May 2015

CITATIONS
2

READS
196

5 authors, including:

Long Chen
Tsinghua University
18 PUBLICATIONS **56** CITATIONS
SEE PROFILE

Yugong Luo
Tsinghua University
85 PUBLICATIONS **408** CITATIONS
SEE PROFILE

Zhaobo Qin
Tsinghua University
15 PUBLICATIONS **32** CITATIONS
SEE PROFILE

Keqiang Li
Tsinghua University
156 PUBLICATIONS **1,600** CITATIONS
SEE PROFILE

EVS28
KINTEX, Korea, May 3-6, 2015

Tire-Road Friction Estimation based on Frequency Characteristics of In-Wheel Electric Drive System

Long Chen, Mingyuan Bian, Yugong Luo, Zhaobo Qin, Keqiang Li
State Key Laboratory of Automotive Safety and Energy, Tsinghua University, Beijing 100084, China,
long-chen12@mails.tsinghua.edu.cn

Abstract

In-wheel drive systems which combine with the permanent magnet synchronous motors (PMSM) and tires are highly electromechanical-coupled. This paper studies the dynamic characteristics of this system to estimate the tire-road friction condition. After a dynamic tire model and a PMSM model is studied, a transfer function from control signal of the motor to the wheel dynamics is obtained. As a result of analyses about longitudinal dynamics in the frequency domains, motor-wheel resonance frequency is observed, which is related to the tire-road friction. Based on this feature, the friction estimation method combining a system identification technique to find dominant resonance frequency and recursive least square filtering, is applied for simulation. The simulation result shows that the proposed approach can detect road friction in the case that the tire is freely rolling, which is not sensitive to the noise and error of wheel speed signal.

Keywords: in-wheel drive, tire-road friction estimation, dynamic tire model, frequency characteristics

1 Introduction

Since the forces between the tires and road interface primarily determine the states of vehicle motion, the knowledge of tire-road friction can be extremely useful for many vehicle active safety control systems, including active roll control (ARC), direct yaw torque control system (DYC), adaptive cruise control system (ACC) and unified chassis control. Particularly, reliable estimation of friction coefficients at each wheel will enable both traction and stability control systems to provide optimum drive/brake torque to the individual wheels so as to maximize traction/brake performances, reduce wheel skid and enhance driving stability. Many researches on vehicle stability control have also proposed the explicit usage of tire-road friction information in determination of the desired yaw rate and other control system variables [1-2].

There are abundant literatures illustrating the state of art of tire-road friction estimation (TRFE), and several different approaches have been proposed, which can be classified into two categories: cause-based and effect-based.

Some researchers try to detect factors that affect the friction coefficient, using optical camera, ultrasonic sensor or other sensors to detect road coverings (such as ice, snow, etc.) so as to estimate the friction coefficient [2].

Effect-based methods directly focus on the vehicle motion effects generated by the determinate control input under certain tire-road friction condition. The effects are shown in the tire as acoustic characteristic, tire-tread deformation and wheel slip. S. Hong, et al. [3] introduced a certain sensor that was fixed to the inner surface of the tire to observe tire deformation. However this method needed a specially equipped sensor and a signal transmitting apparatus. F. Gustafsson [4], and K. Hedrick [5] deemed that the slope between the slip

ratio and friction coefficient curve could give the information. But as the longitudinal tire force can't be accurately estimated by using engine torque or braking pressure, tire forces should be set as measurement vector together with maximum friction coefficient, which makes the Jacobian matrix of the filter complex. As a result, computation load is added on the process of Kalman filter. Meanwhile, when the vehicle is in a normal driving situation, estimated slip ratio is small and sensitive to the noise of wheel speed signal, which results the low accuracy of friction estimation. In a word, there are some limitations about the slope-based method just using time-domain information. E. Ono tried to estimate road condition using the frequency characteristic of wheel speed signals during braking, but it can't be suitable for the driving case [6-7]). M. Bartram found the influence of the tyre/road contact interface on driveline vibrations [8].

While vehicle is traveling, the angular velocity of the wheel can be considered as two parts, namely the high-frequency and low-frequency signals. Slope-based estimation accuracy depends on the tire force and slip ratio, and each parameter can be influenced by the high-frequency signal and static deviation of the lower one. For high-frequency signal, unlike the difficulty to accurately obtain the output torque of engine or braking pressure, in-wheel drive systems combined with PMSM can control and capture the wheel driving torque in high frequency, which may bring a chance to estimate the friction coefficient using high frequency information of wheel speed [9]. But a dynamic motor-wheel model needs to be studied.

This paper focuses on the dynamic characteristics of in-wheel drive system to estimate the tire-road friction coefficient. With a brief review of the traditional concept of longitudinal relaxation length and static tire model, a dynamic tire model for normal driving is introduced. After a PMSM mathematical model is studied, a transfer function from control signal of the motor to the wheel dynamics can be obtained. Then an insight into the longitudinal dynamics in the frequency domains is provided, after local linearization of the wheel spin equations coupled with analytical solution of the transient longitudinal slip formulation is considered. As a result of this analysis, the paper obtains the equation of motor-wheel resonance frequency which is related to the tire-road friction. Based on this feature, the friction estimation method which integrates recursive least square filtering and system identification technique, is proposed only using the information of motor current signal and wheel speed signal. The simulation result shows that the proposed approach can detect friction and it is not sensitive to the noise and sensor error of wheel speed and longitudinal velocity in the case that the tire is freely rolling.

The paper is organized as follows. In Section 2 and 3, a dynamic tire model and a mathematical model of I-PMSM are established. Section 4 illustrates longitudinal dynamics in the frequency domains. Road friction estimation method is introduced in Section 5. Simulation results are presented and analysed in Section 6. Conclusions are given in the end.

2 Tire Model

2.1 Static slip/force models

For the sake of simplicity, only longitudinal motion will be considered in this paper. The dynamics of suspension dynamics, road slope and so on are also neglected. The simplified motion dynamics of a quarter-vehicle model is considered here.

The system is then described as the following form.

$$\begin{aligned} m\dot{v} &= F_x - F_{air} \\ F_{air} &= 0.5 C_d A \rho v^2 \\ I\dot{\omega} &= T_d - F_x R \end{aligned} \tag{1}$$

where m is 1/4 of the vehicle mass and I, R are the inertia and radius of the wheel, respectively. v is the longitudinal velocity of the vehicle, ω is the angular velocity of the wheel, T_d is the driving torque output from the in-wheel motor, and F_x is the tire/road longitudinal friction force.

The most common tire friction models used in the literature are those describing with algebraic slip/force relationships. Slip rate s is defined as

$$s = \begin{cases} \dfrac{R\omega - v}{v} & \textit{for braking} \\ \dfrac{R\omega - v}{R\omega} & \textit{for driving} \end{cases} \tag{2}$$

One of the most well-known models of this type is known as the ''Magic Formula'' model [10]. This model has been shown to suitably match experimental data, obtained under particular conditions of constant linear and angular velocity.

$$F_x = c_1 \sin\left(c_2 \arctan\left(c_3 s - c_4\left(c_3 s - \arctan\left(c_3 s\right)\right)\right)\right) \tag{3}$$

where c_i, $i = 1-4$, are the parameters characterizing this model. They can be identified by matching experimental data, as shown in [10].

Burckhardt [11-12] proposes a simple velocity-independent three-parameter model as follows:

$$F_x = c_1\left(1-e^{-c_2 s}\right)-c_3 s \quad (4)$$

This paper only focuses on the tire force when s is very small for the normal driving case. So Equation (4) can be simplified as

$$F_x = k_s s + F_{x0} \quad (5)$$

Where, F_{x0} is the offset at s =0.

2.2 Dynamic tire model

For relatively low frequency and large wavelength transient and oscillatory vehicle motion, the effect of the finite length of contact patch may be neglected. Some researchers show that the dynamic reaction of the tire force to disturbances can be approximated well using the first order systems. The non-linear relaxation length-based model is used to describe the dynamic longitudinal force F_x^D derived from the steady longitudinal force F_x^S [13].

$$\tau \dot{F}_x^D + F_x^D = F_x^S \quad (6)$$

The time constant τ can be derived from the relaxation length r_x as follows:

$$\tau = \frac{r_x}{v} \quad (7)$$

The relaxation length is the function of the slip ratio s and the wheel load F_z, but the detailed function is too complex to be used in the simulation. Thus a 2-D look-up table revealing the relationship among the computed relaxation length , various values of F_z, and s is presented in Figure 1 [14]**Error! Reference source not found.**. In this study, to minimize the complexity of the calculation process, the non-linear characteristics of the contact patch which is indicated by the speed difference between the leading and trailing part is ignored.

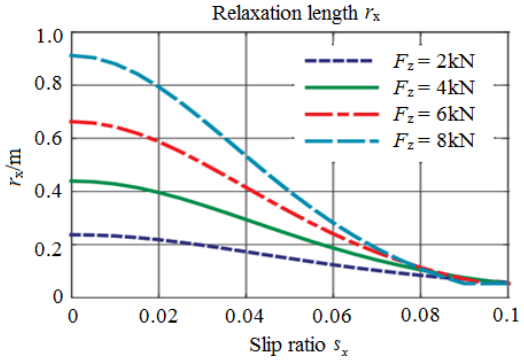

Figure 1: Computed relaxation length characteristics

3 I-PMSM model

The following assumptions are made before establishing the mathematical model of I-PMSM:

1) Neglect the saturation of the electric motor ferrite core.

2) Neglect turbulent flow and hysteresis loss in the electric motor.

3) The currents in the electric motor are symmetrical three-phase sinusoidal currents.

In FOC algorithm, both the three-phase stator A-B-C coordinate system and the two-phase stator α-β coordinate system are the static coordinate systems. While the d-q coordinate system is revolving, the transformations between these three coordinates are given,

$$\begin{pmatrix} i_\alpha \\ i_\beta \end{pmatrix} = \sqrt{\frac{2}{3}} \begin{pmatrix} 1 & -\frac{1}{2} & -\frac{1}{2} \\ 0 & -\frac{\sqrt{3}}{2} & \frac{\sqrt{3}}{2} \end{pmatrix} \begin{pmatrix} i_a \\ i_b \\ i_c \end{pmatrix} \quad (8)$$

$$\begin{pmatrix} i_d \\ i_q \end{pmatrix} = \begin{pmatrix} \cos\theta & \sin\theta \\ -\sin\theta & \cos\theta \end{pmatrix} \begin{pmatrix} i_\alpha \\ i_\beta \end{pmatrix} \quad (9)$$

where i_a , i_b , i_c — a-, b- and c-axis armature currents, i_d , i_q — d- and q-axis armature currents, i_α , i_β — α- and β-axis armature currents, θ — rotor phase.

The torque of the PMSM is determined by i_d and i_q ,

$$T_e = P_n \psi_a i_q + P_n (L_d - L_q) i_d i_q \quad (10)$$

where L_d , L_q — d- and q-axis inductances, P_n — number of pole pairs, ψ_a — permanent magnet flux-linkage, T_e — output torque.

In this study, a surface-mounted PMSM for which L_d equals to L_q , is used. Hence Equation (10) can be simplified as:

$$T_e = P_n \psi_a i_q = K i_q \quad (11)$$

4 Frequency Characteristic

4.1 Transfer function Deduction

Assume that the driving torque includes two kinds of information, low frequency and high frequency, shown as follows.

$$T_d = T_0 + T_1 \sin(2\pi f \cdot t) \quad (12)$$

where T_0 is a constant value, standing for the low frequency information, while $T_1 \sin(2\pi f \cdot t)$ is the high frequency information, T_1 is the amplitude, f means the frequency.

After substituting Equation (12) into Equation (1), the tire dynamic function can be described as Equation (13).

$$I\dot{\omega}=T_0+T_1\sin(2\pi f\cdot t)-F_x^D R \tag{13}$$

With the derivative on both sides of Equation (13), Equation (14) will be obtained as

$$I\ddot{\omega}=2\pi f\cdot T_1\cos(2\pi f\cdot t)-\dot{F}_x^D R \tag{14}$$

Then combine Equation (13) with (14) through multiplying Equation (14) by τ and adding up to Equation (13)

$$\begin{aligned} I\tau\ddot{\omega}+I\dot{\omega}&=T_0+T_1\sin(2\pi f\cdot t)-F_x^D R\\ &+2\pi f\tau\cdot T_1\cos(2\pi f\cdot t)-\tau\dot{F}_x^D R\end{aligned} \tag{15}$$

Considering the dynamic and static tire model (Equation (5) and (6)), the equation above can be simplified as

$$\begin{aligned} &I\tau\ddot{\omega}+I\dot{\omega}=T_0+aT_1\sin(2\pi f\cdot t+\phi)-(k_s s+F_{x0})R\\ &a=\sqrt{1+(2\pi f)^2},\quad \phi=\arctan(2\pi f)\end{aligned} \tag{16}$$

For the driving case, Equation (16) can be written as:

$$I\tau\ddot{\omega}+I\dot{\omega}=T_0+aT_1\sin(2\pi f\cdot t+\phi)-k_s R\frac{R\omega-v}{R\omega}-F_{x0}R \tag{17}$$

Differentiating Equation (17) with respect to time, it can be expressed as:

$$I\tau\dddot{\omega}+I\ddot{\omega}=a2\pi f\cdot T_1\cos(2\pi f\cdot t+\phi)+k_s R\frac{\dot{v}\cdot R\omega-R\dot{\omega}\cdot v}{(R\omega)^2} \tag{18}$$

In this paper, only the normal driving case is studied. The longitudinal vehicle speed is approximately equal to the wheel rotation speed multiplied by effective rolling radius. The derivative of the rotation speed is rather larger than the acceleration of longitudinal velocity, which can be treated as zero. Under these assumption, Equation (18) can be rewritten as:

$$I\tau\dddot{\omega}+I\ddot{\omega}=2\pi fa\cdot T_1\cos(2\pi f\cdot t+\phi)-\frac{k_s R^2}{v}\ddot{\omega} \tag{19}$$

Assume:

$$T_2=T_1\cos(2\pi f\cdot t+\phi) \tag{20}$$

Equation (19) can be rearranged as:

$$I\tau\dddot{\omega}+I\ddot{\omega}+\frac{k_s R^2}{v}\ddot{\omega}=2\pi fa\cdot T_2 \tag{21}$$

With Laplace transform on both sides of Equation (21), it can be written as:

$$I\tau\lambda^3\omega(\lambda)+I\lambda^2\omega(\lambda)+\frac{k_s R^2}{v}\lambda\omega(\lambda)=2\pi faT_2(\lambda) \tag{22}$$

Where, λ is the Laplacian operator.

Then, the transfer function from control signal of the motor to the wheel dynamics can be shown as:

$$\frac{T_2(\lambda)}{\omega(\lambda)}=\frac{I\tau\lambda^3+I\lambda^2+\frac{k_s R^2}{v}\lambda}{2\pi f\sqrt{1+(2\pi f)^2}} \tag{23}$$

But, in practical application, the current of the motor can be measured directly instead of the motor torque. So Equation (23) should be rearranged with Equation (11) as:

$$\frac{i_q(\lambda)}{\omega(\lambda)}=\frac{I\tau\lambda^3+I\lambda^2+\frac{k_s R^2}{v}\lambda}{2\pi fK\sqrt{1+(2\pi f)^2}} \tag{24}$$

So the amplitude ratio between the current and the rotation speed is shown as:

$$\begin{aligned}\frac{A(i_q)}{A(\omega)}&=\left|\frac{i_q(j2\pi f)}{\omega(j2\pi f)}\right|\\ &=\frac{\left|-I(2\pi f)^2+j\left(\frac{k_s R^2}{v}2\pi f-I\tau(2\pi f)^3\right)\right|}{2\pi fK\sqrt{1+(2\pi f)^2}}\\ &=\frac{\left|-I(2\pi f)+j\left(\frac{k_s R^2-Ir_x(2\pi f)^2}{v}\right)\right|}{K\sqrt{1+(2\pi f)^2}}\end{aligned} \tag{25}$$

Assume:

$$b=-I(2\pi f);\ c=\frac{k_s R^2-Ir_x(2\pi f)^2}{v} \tag{26}$$

Then Equation (25) can be expressed as:

$$\frac{A(i_q)}{A(\omega)}=\frac{\sqrt{b^2+c^2}}{K\sqrt{1+(2\pi f)^2}} \tag{27}$$

But the phase relationship between the current and the rotation speed cannot be extracted from Equation (24), due to the phase difference between $T_1\sin(2\pi f\cdot t)$ and T_2. After considering this difference, the phase relationship can be shown as:

$$\varphi(i_q)+\varphi(\omega)=\varphi-\arctan\frac{b}{c}-\frac{\pi}{2}+2\pi k \tag{28}$$

Where k is an integer.

4.2 Motor-wheel resonance frequency

4.2.1 Effect of longitudinal velocity

Figure 2 shows three amplitude ratio-frequency curves under different longitudinal velocities.

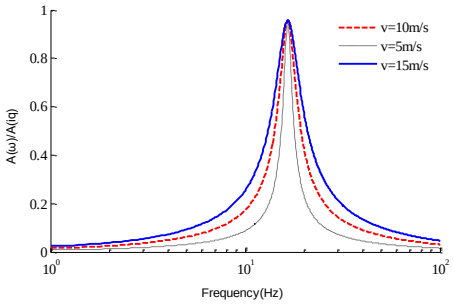

Figure 2: Amplitude ratio under different velocities*

*Parameters for this figure: k_s =60000N; r_x =0.5m; R =0.3m; K =6Nm/A; I =1 kgm^2.

This figure implies that longitudinal velocity affects the curve shape even with identical longitudinal stiffness. But there is a peak point where three curves coincide together in Figure 2, which means it will be not influenced by velocity.

The frequency of the peak point is called as motor-wheel resonance frequency in this paper.

4.2.2 Motor-wheel resonance frequency

The motor-wheel resonance frequency cannot be obtained directly from Equation (24). From Figure 2, it shows that the empirical value of resonance frequency is over 10 Hz.

With this empirical value, approximate conversion can be made on Equation (25).

$$\begin{aligned}\min[\frac{A(i_q)}{A(\omega)}] &= \min[\frac{\left|-I(2\pi f)+j\left(\frac{k_s R^2 - Ir_x(2\pi f)^2}{v}\right)\right|}{K\sqrt{1+(2\pi f)^2}}] \\ &\approx \min[\frac{\left|-I(2\pi f)+j\left(\frac{k_s R^2 - Ir_x(2\pi f)^2}{v}\right)\right|}{K\cdot 2\pi f}] \\ &= \min[\left|\frac{-I}{K}+j\left(\frac{k_s R^2/2\pi f - Ir_x(2\pi f)}{vK}\right)\right|]\end{aligned} \quad (29)$$

After some mathematical deduction, motor-wheel resonance frequency can be expressed as:

$$f_0 \approx \frac{R}{2\pi}\sqrt{\frac{k_s}{Ir_x}} \quad (30)$$

Apparently, Equation (30) explains the regular patterns shown in Figure 2 that the motor-wheel resonance frequency is unrelated to velocity. R , I , r_x are considered as constants in an instant, so if the resonance frequency can be obtained, then the longitudinal stiffness k_s can be estimated by Equation (30). As described in Introduction, the longitudinal stiffness k_s , namely the slope of F_x verse s curve, has a linear relationship to the friction coefficient. As a summary of this section, it is possible to estimate friction coefficient using the frequency characteristic of wheel and motor. Due to the characteristic of the motor-wheel resonance frequency which is unrelated to velocity, this idea of TRFE above can overcome the shortcoming of traditional method that is sensitive to velocity estimation error.

5 Frequency-based Road friction estimation

As discussed in Section 4, tire road friction coefficient can be estimated by the motor-wheel resonance frequency. So this paper proposes a estimating process as follows:

Step 1: with system identification theory, the resonance frequency of the motor-wheel system is obtained;

Step 2: based on Equation (30), tire stiffness is observed using the approach of recursive least squares(RLS);

Step 3: as there is a linear relationship between longitudinal stiffness and friction coefficient, the latter one can be estimated by an equation which express this relationship.

The whole scheme of friction estimation is shown as Figure 3.

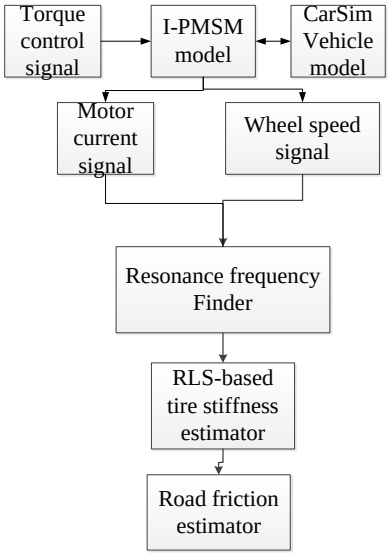

Figure 3: scheme of road friction estimator

5.1 Resonance frequency finder

5.1.1 Problem formulation

In this paper, a problem to estimate a dominant frequency of motor-wheel system is considered. It is assumed that motor-wheel system can be described by a 2nd-order vibration system $P(z)$, shown in Figure 4.

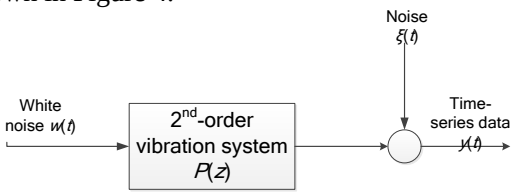

Figure 4: time-series modelling

From Figure 4, $P(z)$ is driven by white noise $w(t)$, namely the current signal of the motor. Moreover, the measure time-series data $y(t)$, namely the wheel speed signal, is contaminated by observation noise $\xi(t)$ which is assumed to be white-Gaussian. Then time-series data $y(t)$ is expressed as:

$$y(t)=P(z)w(t)+\xi(t) \quad (31)$$

5.1.2 Estimation procedure

In this sub-section, an estimation method of a dominant resonance frequency which incorporates system identification technique into time-series analysis is briefly summarized [15]. In this method, high-order time-series analysis is applied to the time-series model and the time-series data $y(t)$, and the input is reconstructed from the high-order time-series model and time-series data $y(t)$. Next, a band-pass filtering is applied to the reconstructed input-output data, then 2nd order ARX(Auto-Regressive eXogenous) model is estimated by system identification theory. The resonance frequency is estimated from coefficients of denominator of the estimated ARX model.

The procedure of the method is summarized as follows.

Step 1 Fitting to AR model

Time-series data $y(t)$ is fitted to a high-order (ex. 20th or 30th) AR model.

$$A(q)y(t)=w(t) \tag{32}$$

where $w(t)$ is the driving white noise, and $A(q)=1+a_1q^{-1}+\cdots+a_nq^{-n}$.

By using the least-squares method, the estimate $\hat{A}(q)$ is obtained.

Step 2: reconstruction of input data.

From $y(t)$ and the estimated $\hat{A}(q)$, $\hat{w}(t)$ is reconstructed as follows.

$$\hat{w}(t)=\hat{A}(q)y(t) \tag{33}$$

Step 3: system identification with ARX model.

System identification is applied to the system whose input is $\hat{w}(t)$ and output is $y(t)$. As data pre-processing, a band-pass filtering whose band-pass includes the dominant resonance frequency of the system is applied to both input data and output data.

Then, 2nd order ARX model

$$A_L(q)y(t)=B_L(q)\hat{w}(t)+\xi(t) \tag{34}$$

is estimated, where

$$A_L(q)=1+a_1q^{-1}+a_2q^{-2} \tag{35}$$

$$B_L(q)=b_1q^{-1}+b_2q^{-2} \tag{36}$$

and $\xi(t)$ is the equation error.

Step 4 calculation of resonance frequency

Characteristic roots $\lambda_i(i=1,2)$ of $A_L(q)$ are computed. Then the resonance frequency $\hat{f}_0$ is estimated as

$$f_0=\frac{\sqrt{d_i^2-c_i^2}}{2\pi} \tag{37}$$

where c_i and d_i are computed by

$$c_i=\frac{\ln\left(\mathrm{Re}(\lambda_i)^2+\mathrm{Im}(\lambda_i)^2\right)}{2\Delta T} \tag{38}$$

$$d_i=-\frac{1}{2\Delta T}\frac{\mathrm{Im}(\lambda_i)}{\mathrm{Re}(\lambda_i)} \tag{39}$$

ΔT is the sampling time.

5.2 RLS-based tire stiffness estimator

By Equation (30), the slip slope k_s is determined by the resonance frequency.

According to the estimated resonance frequency, the slip slope can be estimated by the RLS method. The RLS method can be described by the following equation:

$$x(t)=\vartheta^T(t)\varepsilon(t)+e(t) \tag{40}$$

where $\varepsilon(t)$ is the estimated parameter, which is slip slope k_s in this research. $x(t)$ is the square motor-wheel resonance frequency $f_0^2(t)$ and $e(t)$ is the error. $\vartheta(t)$ is the regression vector, which is $\frac{R^2}{4Ir_x\pi^2}$.

The RLS algorithm has the procedure as follows at each time step [16]:

Step 1: Get the measurement value of the system output $x(t)$ and determine the regression vector $\vartheta(t)$.

Step 2: According to the difference between system actual output at present time step and the system output predicted in the previous time step, determine the error $e(t)$:

$$e(t)=x(t)-\vartheta^T(t)\varepsilon(t-1) \tag{41}$$

Step 3: The update gain vector $K(t)$ can be calculated as:

$$K(t)=\frac{P(t-1)\vartheta(t)}{\chi+\vartheta(t)^TP(t-1)\vartheta(t)} \tag{42}$$

And the covariance matrix $P(t)$ can be calculated by:

$$P(t)=\frac{1}{\chi}\left[P(t-1)-\frac{P(t-1)\vartheta(t)\vartheta^T(t)P(t-1)}{\chi+\vartheta(t)^TP(t-1)\vartheta(t)}\right] \tag{43}$$

Step 4: Update the estimated parameter

$$\varepsilon(t)=\varepsilon(t-1)+K(t)e(t) \tag{44}$$

χ is called the forgetting factor, which is within the scope of (0.9, 1).

5.3 Road friction estimator

When the slip slope k_s is estimated, based on the experimental data in the simulation, the tire-road friction coefficient can be estimated by the following equation:

$$\mu_{\max} = a_{\mu_{\max}} k_s + b_{\mu_{\max}} \quad (45)$$

Where $a_{\mu_{\max}}$ =0.00001, $b_{\mu_{\max}} = -0.2$.

6 Simulation

Aiming at simulating the dynamics reactions of four-wheel-independent drive electric vehicle under different driving inputs, the wheels are disconnected from the engine in the CarSim model, while the torque signals output from the PMSM model in Simulink is input to the wheels in CarSim.

In this simulation, the motor torque demand is applied at the beginning as the following figure. The input traction torque is shown in Figure 5. The longitudinal stiffness is set as 60000N in the vehicle dynamics model, so the corresponding friction coefficient is 0.4. Other parameters are set as: τ_x =0.5m; R =0.3m; I =1 kgm^2.

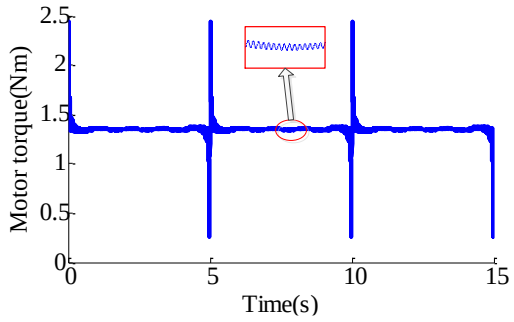

Figure 5: motor torque demand

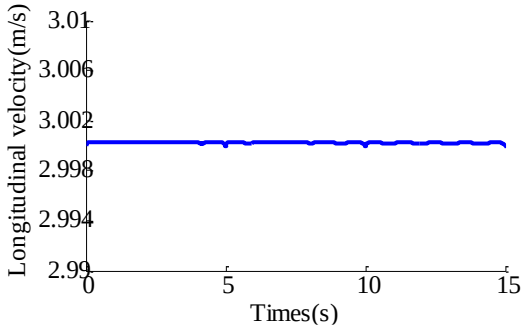

Figure 6: longitudinal velocity

Figure 6 shows the actual vehicle velocity. At 5s, the motor torque is changing violently. However, longitudinal velocity only changes a little, which proves that the influence factors of velocity on the frequency response can be ignored, and the deduction procedure in Section 4.1 is reasonable.

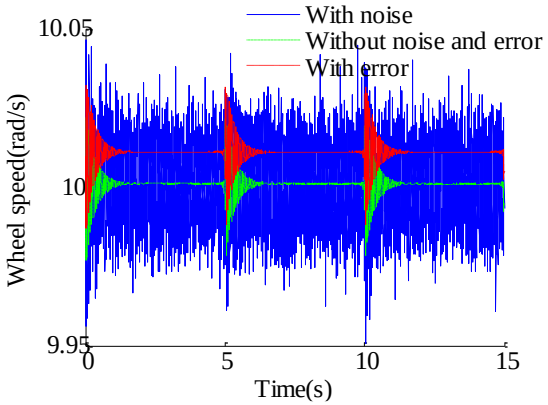

Figure 7: wheel speed

Figure 7 compares different wheel speed data. The dot-dashed line is the data output from CarSim vehicle model, without noise and error. The line changes its shape along with the motor torque demand. The dashed line is the data output from CarSim vehicle model plus a constant error, which is used to check the sensitivity to wheel speed static error in estimation methods. Similarly, the solid line is the true wheel speed plus a white noise to check the sensitivity to the noise of wheel speed sensor. It can be seen that the true wheel speed is shaded by the noise.

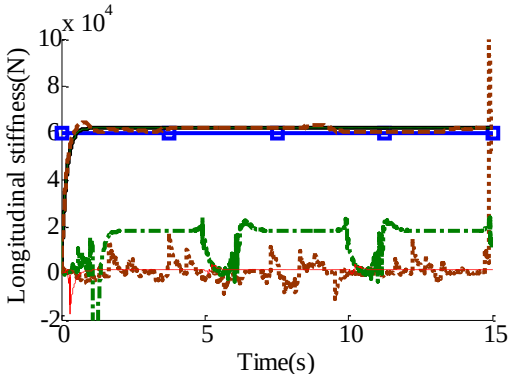

Figure 8: Longitudinal stiffness*

*Legend for Figure 8:

Slope-Kalman-based estimated value with noise
Slope-Kalman-based estimated value without noise and error
Reference value
Slope-Kalman-based estimated value with error
Frequency-based estimated value without noise and error
Frequency-based estimated value with error
Frequency-based estimated value with noise

Figure 8 compares the estimated longitudinal stiffness of proposed frequency-based method and the well-known slope-Kalman-based approach under different signals. It shows that all the estimation results of frequency-based method which is proposed in this paper are acceptable for three cases, which indicates this method is not sensitive to sensor noise and unknown static error. As a comparison, even though there is no noise and error in the wheel speed signal, the well-

known slope-Kalman-based method cannot work well since it neglects the dynamic property of tire. For the dot-dashed line, at this time interval between 5s and 6s when the wheel speed is changing violently, the traditional approach even cannot work. It is also shown in this figure, that traditional method (slope-Kalman-based method) is sensitive to sensor noise and unknown static error.

To verify the robustness of proposed estimator stated above, fast Fourier transform [17] is introduced to get the amplitude of wheel speed for different frequencies, which is shown as Figure 9.

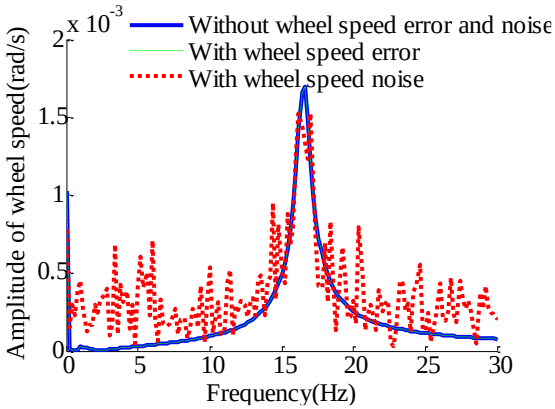

Figure 9: amplitude of wheel speed

In Figure 9, it shows the amplitude-frequency curve with static error coincides exactly with the one with no error. However, the sensor noise has influence on the shape of the curve, but for the resonance frequency, only a little bias exists between two curves with and without noise. So this figure verifies the robustness of proposed estimator to the wheel speed noise and error. Combining the results of Figure 8 and 9, the equation of motor-wheel resonance frequency deduced in Section 4 is accurate to estimate the longitudinal tire stiffness.

Comparing Figure 9 and Figure 2, although the velocities are different, the resonance frequency shown in Figure 9 is the same with the one Figure 2 with $k_s = 60000N$. It proves the discussion in Sub-section 4.2.1 that resonance frequency is unrelated to velocity, which can further verify correctness of the deduction procedure and the equation of motor-wheel resonance frequency. Also, the robustness of proposed estimator to velocity error and noise can be guaranteed by this feature of resonance frequency.

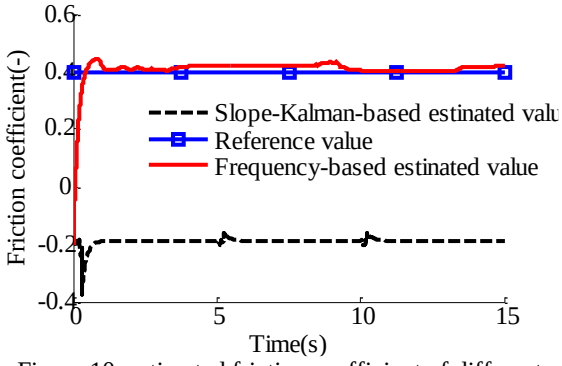

Figure 10: estimated friction coefficient of different approaches

In Figure 10, the estimated friction coefficient with the proposed approach is much more accurate and steady than the one with the traditional method. The convergence time is 1s.

7 Conclusion

This paper tries to estimate the tire-road friction coefficient by considering the dynamic characteristics of in-wheel drive system. Combining dynamic tire model with PMSM mathematical model, a transfer function from control signal of the motor to the wheel dynamics can be obtained. Then an insight into the longitudinal dynamics in the frequency domains is provided. As a result of these analyses, motor-wheel resonance frequency, which is related to the tire-road friction, is observed. Based on this feature, a frequency-based road friction estimation method including resonance frequency finder and recursive least square is applied to simulation under a set of high frequency torque demands injected to the motor in MATLAB/Simulink. The simulation results show that the proposed approach can detect friction in the case that the tire is freely rolling only using the information of wheel speed signal.

Contribution of this paper:

- A transfer function from control signal of the driving motor to the wheel dynamics is obtained;
- Based on the feature of resonance frequency, a road friction estimation method only using the information of wheel speed signal is proposed, which is not sensitive to the noise and sensor error of wheel speed and longitudinal velocity.

This article only focuses on the small slip ratio case. The lateral motion as well as combined longitudinal/lateral dynamics are left for future investigation.

Acknowledgments

The authors are grateful for the sponsorship from the National Key Fundamental Research Program of China (Grant No. 2011CB711204).

References

[1] R. Rajamani, *vehicle dynamics and control*, ISBN 978-1-4614-1432-2, New York, Springer US, 2005.

[2] M. Yanada, et al, *road surface condition detection technique based on image taken by camera attached to vehicle rearview mirror*, Review of Automotive Engineering, ISSN 1349-4740, 22 (2005), 163-168.

[3] S. Hong, G. Erdogan, K. Hedrick, and F. Borrelli, *tyre–road friction coefficient estimation based on tyre sensors and lateral tyre deflection: modeling, simulations and experiments*, Vehicle System Dynamics, ISSN 0042-3114, 51(2013), 627-647.

[4] F. Gustaffson, *slip-based tire-road friction estimation*, Automatica, ISSN 0005-1098, 33(1997), 1087–1099.

[5] C. Lee, K. Hedrick, K. Yi, *real-time slip-based estimation of maximum tire-road friction coefficient*, IEEE/ASME Transactions on Mechatronics, ISSN 1083-4435, 9(2004), 454 – 458,.

[6] T. Umeno, *et al*., *estimation of tire-road friction using tire vibration model*, SAE Technical Papers, 2002-01-1183.

[7] E. Ono, *et al*., *estimation of automotive tire force characteristics using wheel velocity*, Control Engineering Practice, ISSN 0967-0661,11(2003), 1361-1370.

[8] M. Bartram, *et al*., *a study on the effect of road friction on driveline vibrations*, Proceedings of the Institution of Mechanical Engineers, Part K: Journal of Multi-body Dynamics, ISSN 14644193, 224(2010), 321-340.

[9] N. Mutoh, *front-and-rear-wheel-independent-drive type electric vehicle (FRID EV) with the outstanding driving performance suitable for next-generation electric vehicles*, 2012 IEEE International Electric Vehicle Conference, ISBN 9781467315623, 2012.

[10] H. B. Pacejka, *tyre and vehicle dynamics*, ISBN 9780750669184, Oxford, Butterworth-Heinemann, 2002.

[11] C. Canudas-de-Wit, *et al., dynamic friction models for road/tire longitudinal interaction*, Vehicle System Dynamics, ISSN 0042-3114, 39(2003), 189-226.

[12] J. Yi, *on the hybrid physical/dynamic tire/road friction model*, ISBN 9780791848920, New York, American Society of Mechanical Engineers, 2010.

[13] de Wit, Carlos Canudas, *et al., dynamic tire friction models for vehicle traction control*, Proceedings of the IEEE Conference on Decision and Control, ISSN 01912216, 4(1999), 3746-3751.

[14] J. Adcox, *et al., interaction of anti-lock braking systems with tire torsional dynamics*, Tire Science and Technology, ISSN 0090-8657, 40(2012), 171-185.

[15] T. Hirao, *et al., Resonance frequency estimation of time-series data by subspace method*, Proceedings of the ICROS-SICE International Joint Conference 2009, ISBN 9784907764333, 4913-4916.

[16] B. Li, *et al., a novel cost effective method for vehicle tire-road friction coefficient estimation*, 2013 IEEE/ASME International Conference on Advanced Intelligent Mechatronics (AIM), ISBN 9781467353199, 2013, 1528-1533.

[17] P. Duhamel, M. Vetterli, *fast fourier transforms: a tutorial review and a state of the art*, Signal Processing, ISSN 01651684, 19(1990) 259-299.

Authors

Long Chen received the B.Tech. degree in automotive engineering from Jilin University, Changchun, China, in 2012. He is currently working toward the Ph.D. degree in automotive engineering at the Tsinghua University.

His research interests include advanced control system design, observer design for nonlinear systems, system identification, and evaluation of automotive safety technology.

Mingyuan Bian received the B.Tech. and the Ph.D. degree from Beijing Institute of Technology, Beijing, China, in 1991 and 2003. And ever worked as a Postdoctoral fellow in Tsinghua University since 2003 to 2005.

He is currently an Associate Professor with the Department of Automotive Engineering, Tsinghua University. He has authored more than 40 journal papers. He is the co-holder of 10 patent applications. His research interests include vehicle and electric vehicle dynamics and control.

Yugong Luo received the B.Tech. and M.S. degrees from Chongqing University, Chongqing, China, in 1996 and 1999, respectively, and the Ph.D. degree from Tsinghua University, Tsinghua, China, in 2003.
He is currently an Associate Professor with the Department of Automotive Engineering, Tsinghua University. He has authored more than 80 journal papers. He is the co-holder of 29 patent applications. His research interests include vehicle and electric vehicle dynamics and control.

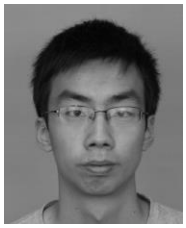

Zhaobo Qin received the B.Tech. degree in Department of Precision Instrument at Tsinghua University, China, in 2013. He is currently working towards the Ph.D. degree in automotive engineering at Tsinghua University.
He is now doing research in hybrid electric vehicle and the powertrain system.

Keqiang Li received the B.Tech. degree from Tsinghua University, Tsinghua, China, in 1985 and M.S. and Ph.D. degrees from Chongqing University, Chongqing, China, in 1988 and 1995, respectively.
He is currently a Professor with the Department of Automotive Engineering, Tsinghua University. He served on the Editorial Boards of the International Journal of ITS Research and the International Journal of Vehicle Autonomous Systems. He has authored more than 100 papers.
He is the holder of 32 patents in China and Japan. His research interests include vehicle dynamics and control for driver-assistance systems and hybrid electrical vehicles.

Dr. Li has served as a Senior Member of the Society of Automotive Engineers of China. He was the recipient of the "Changjiang Scholar Program Professor" title and several other awards from public agencies and academic institutions in China.

Appendix

Table 1: List of symbols

Symbols	Meaning	Unit
R	Effective rolling radius	m
m	1/4 of the vehicle mass	kg
I	inertia of the wheel	kgm^2
v	longitudinal velocity of the vehicle	m/s
ω	angular velocity of the wheel	rad/s
T_d	driving torque output from the in-wheel motor	Nm
F_x	tire/road longitudinal friction force	N
F_{air}	Air drag force	N
C_D	drag coefficient	-
A	wind area	m^2
ρ	Air density	kg/m^3
s	slip ratio	-
c_i	$i=1-4$, parameters characterizing this model	-
k_s	the slope of the F_x versus s curve at s =0, or longitudinal stiffness	N
F_{x0}	the longitudinal force offset at s =0	N
F_x^D	dynamic longitudinal force	N
F_x^D	steady longitudinal force	N
τ	time constants	s
r_x	relax length of tire	m
i_a, i_b, i_c	a-, b- and c-axis armature currents	A
i_d, i_q	d- and q-axis armature currents	A
i_α, i_β	α- and β-axis armature currents	A
θ	rotor phase	rad
L_d, L_q	d- and q-axis inductances	mH
P_n	number of pole pairs	-
Ψ_a	permanent magnet flux-linkage	
T_e	output torque	
K	Torque constant	Nm/A
T_0	a constant torque value	Nm
T_1	amplitude of high-frequency torque	Nm
f	frequency of high-frequency torque	Hz
a,b,c,ϕ,T_2	symbols used to simplify the	-

	deduction	
λ	Laplacian operator	-
$A(i_q)$	amplitude of i_q	A
$A(\omega)$	amplitude of ω	rad/s
$\varphi(i_q), \varphi(\omega)$	phase of i_q and ω	rad
k	an integer	-
f_0	motor-wheel resonance frequency	Hz
f_e	fundamental frequency of PMSM	Hz
v_0	motor-wheel resonance velocity	m/s
$y(t)$	time-series output data of wheel-motor system	
$P(z)$	The transfer function of wheel-motor system	
$w(t)$	the driving white noise	
$\hat{w}(t)$	Reconstructed input data	
$A(q)$	regression vector in "Resonance frequency finder"	
$\hat{A}(q)$	The estimated regression vector in "Resonance frequency finder"	
$A_L(q), B_L(q)$	The vector in 2nd order ARX model	
a_i	Coefficients in $A(q)$	
b_i	Coefficients in $B_L(q)$	
$\hat{w}(t)$	Reconstructed input data	
d_i, g_i	symbols used to simplify the computation of $\hat{f}_0$	
$\hat{f}_0$	The estimated resonance frequency	
λ_i	$i = 1, 2$, characteristic roots of $A_L(q)$	
ΔT	the sampling time	
$\xi(t)$	observation noise	-
$x(t)$	output data in the RLS method	
$\varepsilon(t)$	the estimated parameter in the RLS method	
$e(t)$	the error in the RLS method	
$\vartheta(t)$	regression vector in the RLS method	
$K(t)$	update gain vector in the RLS method	
$P(t)$	covariance matrix in the RLS method	
χ	the forgetting factor in the RLS method	
$\mu_{\max}$	Road friction coefficient	-
$a_{\mu_{\max}}, b_{\mu_{\max}}$	Coefficient in Equation (48)	-